

Accurate Heart Rate Monitoring During Physical Exercises Using PPG

Andriy Temko, *Senior Member, IEEE*

Abstract—Objective: The challenging task of heart rate (HR) estimation from the photoplethysmographic (PPG) signal, during intensive physical exercises is tackled in this paper. **Methods:** The study presents a detailed analysis of a novel algorithm (WFPV) that exploits a Wiener filter to attenuate the motion artifacts, a phase vocoder to refine the HR estimate and user-adaptive post-processing to track the subject physiology. Additionally, an offline version of the HR estimation algorithm that uses Viterbi decoding is designed for scenarios that do not require online HR monitoring (WFPV+VD). The performance of the HR estimation systems is rigorously compared with existing algorithms on the publically available database of 23 PPG recordings. **Results:** On the whole dataset of 23 PPG recordings, the algorithms result in average absolute errors of 1.97 and 1.37 BPM in the online and offline modes, respectively. On the test dataset of 10 PPG recordings which were most corrupted with motion artifacts, WFPV has an error of 2.95 BPM on its own and 2.32 BPM in an ensemble with 2 existing algorithms. **Conclusion:** The error rate is significantly reduced when compared with the state-of-the art PPG-based HR estimation methods. **Significance:** The proposed system is shown to be accurate in the presence of strong motion artifacts and in contrast to existing alternatives has very few free parameters to tune. The algorithm has a low computational cost and can be used for fitness tracking and health monitoring in wearable devices. The Matlab implementation of the algorithm is provided online.

Index Terms—Photoplethysmographic, spectrum estimation, heart rate, Wiener filter, phase vocoder, Viterbi decoding.

I. INTRODUCTION

WEARABLE devices have gradually increased their functionality over the last decades. Modern wearable devices are equipped with a number of internal and external sensors and can offer many useful fitness tracking features such as counting steps, calories, tracking sleep, etc. Photoplethysmography (PPG) based heart rate (HR) monitoring during physical exercise is one of these features [29, 30]. Implemented in smart-watches or wristbands, HR monitoring can guide exercisers to adapt their training load and better match their training goals [26]. PPG signals have become a popular alternative to traditional Electrocardiography (ECG) based HR estimation which measures the bio-potential generated by electrical signals that control the expansion and contraction of heart chambers. However, ECG requires the presence of ground and reference sensors that must be attached to the chest. PPG-based HR monitoring at the peripheral

positions such as earlobes, fingertips or wrists is seen as a much more convenient solution.

The PPG signals [29, 30, 1-3] come from PPG sensors which are embedded in these wearable devices. A PPG sensor emits light to the skin and measures the changes of intensity of the light which is reflected or transmitted through the skin. The periodicity of these measurements in most cases corresponds to the cardiac rhythm, and thus, HR can be estimated from the PPG signal.

Motion artifacts (MAs) are known to be a limiting factor that prevents the straight-forward usage of PPG, especially in free living conditions. MAs are considered to result from sensor-tissue motion and sensor deformation. Strong movements during physical exercise make the HR estimate inaccurate as shown in Fig. 1. Due to motion the sensors might situate far enough apart from the skin that the true HR peak is absent in the PPG spectrum. A number of methods have been proposed to detect, remove or attenuate MAs in PPG signals, including adaptive filtering [4, 5, 22, 25], independent component analysis [6], empirical mode decomposition [7, 23] or other decomposition models [3, 27], spectral subtraction [8, 21, 24], and Kalman filtering [9].

A three-stage TROIKA method has recently been proposed to estimate HR from PPG signals for scenarios where MAs are strong [2]. The method was based on signal decomposition, sparsity-based high-resolution spectrum estimation, and spectral peak tracking and verification. The average absolute error of 2.34 beats per minute (BPM) was reported on 12 PPG recordings. The TROIKA method was enhanced in [3] where the spectra of PPG and acceleration signals were jointly estimated using a common sparsity constraint on the spectral coefficients (JOSS). This was achieved by means of a multiple measurement vector model [10]. The error was reduced to 1.28 BPM when evaluated on the same 12 PPG recordings.

For the IEEE Signal Processing Cup 2015 the database of 23 PPG recordings of people running on a treadmill or doing intensive physical exercises was made public (<http://zhilinzhang.com/spcup2015/data.html>). The evaluation rules and metrics are defined which facilitates the comparison between different approaches. In the period since the provision of this dataset, several HR estimation algorithms have been designed and tested [2, 3, 21-25]. However, the reported improvements in performance are usually accompanied with

The preliminary results of this study have been presented at EMBC 2015 and ICASSP 2017. This work was supported in part by a Science Foundation Ireland Research Centre Award (12/RC/2272) and WT Seed Award (200704/Z/16/Z).

A. Temko is with Irish Centre for Fetal and Neonatal Translational Research (INFANT), Dept. Electrical and Electronic Engineering, University College Cork, Ireland, atemko@ucc.ie

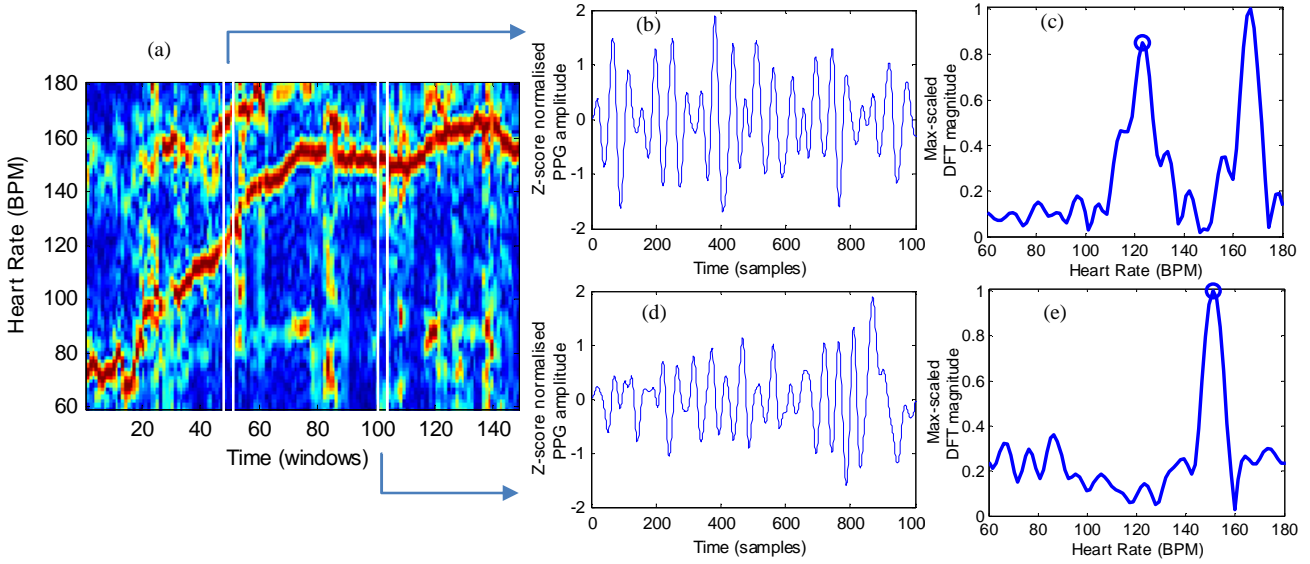


Fig. 1. The challenge of HR estimation during physical exercises. Plot (a) shows a spectrogram of a 5min PPG recording. Plots (b) and (d) show examples of a PPG signal from the spectrogram in (a). Plot (c) and (e) show the spectral envelopes of the PPGs in (b) and (d), respectively. The true HR is denoted with a circle. In the presence of MAs, plots (b) and (c), the highest peak of the spectral envelope does not coincide with the true HR. Best viewed in color.

the increased number of free parameters which may be a sign of overfitting given the fixed size of the dataset on which the algorithms are both designed and tested.

In this paper a new approach to HR estimation which is based on Wiener filtering and the phase vocoder is detailed. In contrast to the previously presented systems, the proposed solution does not rely on a set of heuristic rules and thresholds and requires very few parameters to be tuned. The noise signature is estimated from accelerometer signals and the Wiener filter is used to attenuate the noise components in the PPG signal. The phase vocoder is exploited to overcome the limited resolution of the discrete Fourier transform and to refine the initial dominant frequency estimation. A user-adaptive post-processing step is introduced and additionally an offline version of post-processing which is based on Viterbi decoding is proposed that requires no tunable parameters.

The main contributions of this study are:

- 1) A detailed description of the HR estimation algorithm (WFPV) including the proposed user-adaptive post-processing
- 2) An offline version that uses Viterbi decoding is designed (WFPV+VD) for applications where online HR monitoring is not required (e.g. for fitness trackers for swimmers or offline fitness statistics). A significantly higher performance is obtained by trading online monitoring for accuracy.
- 3) The performance of the most accurate alternatives published to date is summarised and thoroughly compared with both the online WFPV and offline WFPV+VD.
- 4) Benefits of combining different HR estimation algorithms are discussed and an ensemble is designed. Its superior

performance is presented for the first time.

5) The Matlab implementation of the designed HR estimation algorithms is made available through online resources.

The paper is organized as follows. The developed system is described in detail in Section II. Section III describes the database, metrics and the performance assessment routine used in the study. The results on the provided data are presented in Section IV and conclusions are drawn in Section V.

II. HEART RATE ESTIMATION ALGORITHM

The flowchart of the developed system is shown in Fig. 2. The system consists of 4 main blocks – pre-processing, signal de-noising to attenuate the influence of MAs, HR estimation, and post-processing. The examples of signal transformations carried out at each stage are illustrated in Fig. 3.

A. Preprocessing

During the preprocessing stage, the two PPG signals and three accelerometer signals are filtered with a 4th order Butterworth band-pass filter (0.4-4 Hz) as shown in Fig. 3(a). The two PPG signals are then normalized to zero mean and unit variance (z-score normalization) and averaged. The averaged PPG signal and the 3 accelerometer signals are down-sampled from 125 to 25Hz for further processing. The signals are then subjected to the Discrete Fourier Transform (DFT) with the number of bins set to 1024. Fig. 3 (b) shows the spectral envelope of the PPG signal for HRs ranging from 60 to 180 BPM. This range of HRs is chosen based on the specifics of database used in this study



Fig. 2. The flowchart of the developed HR estimation system.

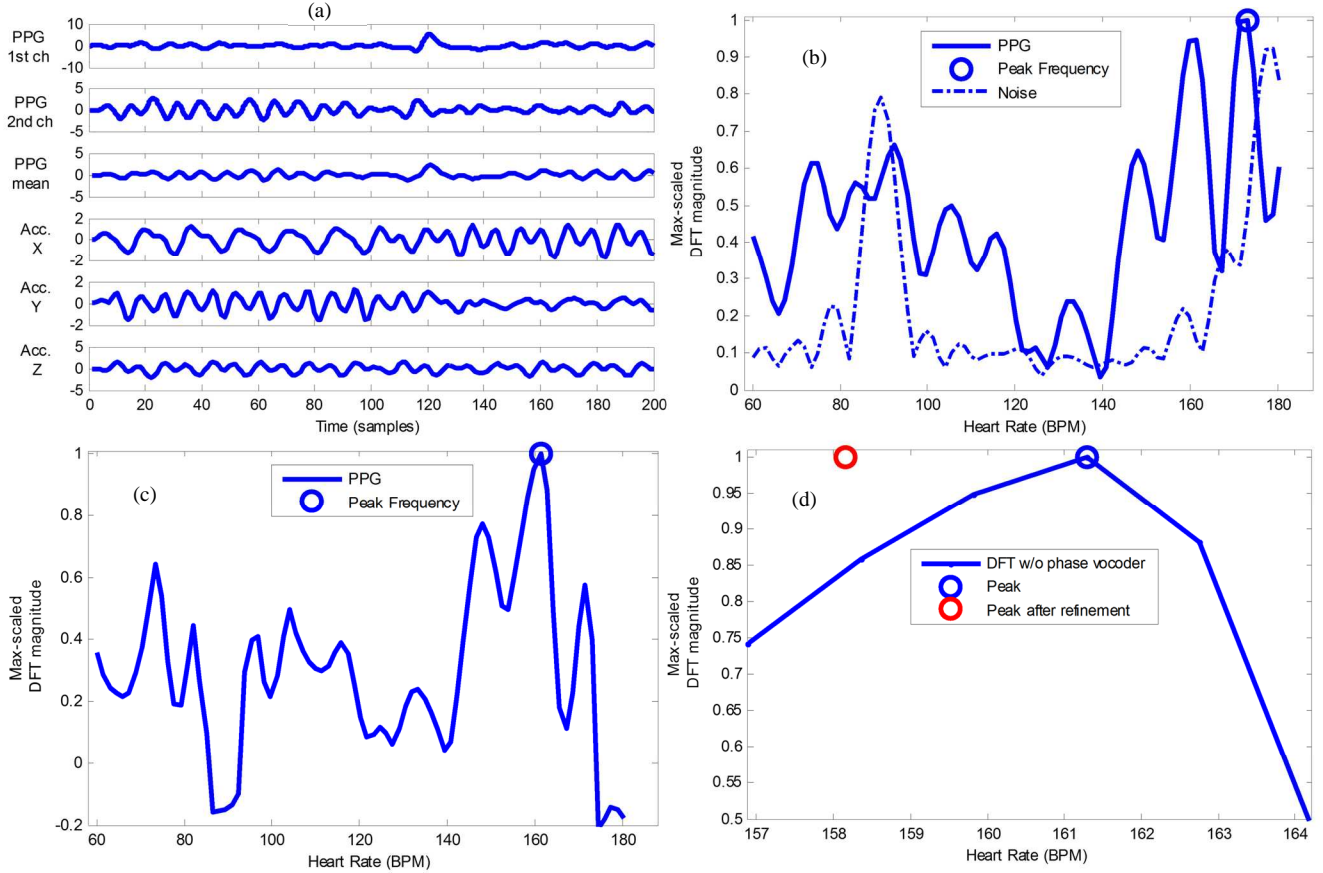


Fig. 3. Signal transformation in the developed WFPV system. Plot (a) shows z-score normalised PPG from two channels, average PPG, and three accelerometer signals after filtering; (b) shows the spectral envelopes of PPG and noise, measured as average accelerometer signals, and the peak frequency of the PPG, (c) shows the processed spectral envelope and its maximum after MAs were attenuated with Wiener filtering; (d) shows the maximum of the spectral envelope before and after the phase vocoder.

which will be explained in Section III and can be changed accordingly for other corpses. Overall, the pre-processing stage in this work repeats that of other papers that report results on this dataset [1, 3, 6].

B. De-noising using Wiener filtering

The Wiener filter is a common tool to estimate a desired signal by linear time-invariant filtering of an observed noisy process [15, 31]. Assuming known stationary signal and additive noise spectra, the Wiener filter performs the minimum mean square error estimation of the desired signal given another related process. Causal Wiener filtering is applied here to estimate the clean PPG signal from the observed PPG signal. The noisy PPG signal, $X(f)$, is assumed to be corrupted by additive MA noise:

$$X(f) = S(f) + N(f) \quad (1)$$

where $S(f)$ and $N(f)$ are the spectra of the clean PPG signal and the MAs, respectively. The estimation of the clean signal can then be obtained as:

$$\tilde{S}(f) = X(f) - N(f) = \left(1 - \frac{N(f)}{X(f)}\right) X(f) = W(f)X(f) \quad (2)$$

For a signal observed in uncorrelated additive random noise, the

frequency-domain Wiener filter is given as:

$$W(f) = \frac{P_{XX}(f) - P_{NN}(f)}{P_{XX}(f)} = \frac{P_{SS}(f)}{P_{SS}(f) + P_{NN}(f)} \quad (3)$$

where $P_{SS}(f)$, $P_{NN}(f)$ and $P_{XX}(f)$ are the power spectrums of the clean signal, noise and observed signal. The filter convolution in time domain is equivalent to multiplication in frequency and thus the Wiener filter acts as an adaptive signal-to-noise dependent attenuator, where frequencies which are more affected by the noise are given less importance.

The filter (Eq. 3) requires separate estimates of the noise and signal power spectrums. The noise spectrum can be directly estimated from the accelerometer signals which is done by averaging the spectrum of the 3 accelerometer signals. The clean PPG spectrum, $P_{SS}(f)$, can be estimated as a subtraction of the noise signal from the observed signal, $P_{XX}(f) - P_{NN}(f)$, or recursively from previous filter outputs. Depending on how the power spectrum of the clean PPG signal is estimated, two Wiener filters are implemented, with frequency domain filter coefficients given as:

$$w_1(t, k) = 1 - \frac{P_{NN}(t, k)}{\frac{1}{C} \sum_{i=t-C+1}^t P_{XX}(i, k)} \quad (4)$$

$$w_2(t, k) = \frac{\frac{1}{C} \sum_{i=t-C}^{t-1} w_2(i, k) P_{XX}(i, k)}{\frac{1}{C} \sum_{i=t-C}^{t-1} w_2(i, k) P_{XX}(i, k) + P_{NN}(t, k)} \quad (5)$$

where $w(t, k)$ is the weight of the k -th frequency bin at time, t . The power spectrums of noise and PPG in Eq. 5 and Eq. 6 are normalized by their maximum values to be commensurable. It can be seen that in both equations the power spectrum of the observed signal is averaged over the past C spectral envelopes ($C=15$, in this work). In Eq. 4, the power spectrum of the clean PPG signal is estimated by subtracting the observed noise from the observed PPG signal. If $C=1$, then the Wiener filter in Eq. 4 performs a simple version of spectral subtraction [16, 17]. In Eq. 5, the spectrum of the clean PPG signal is computed recursively by averaging the previous filtered signal outputs.

The spectral envelop of the cleaned PPG signal is then obtained by multiplying the spectral envelope of the observed signal, $P_{XX}(t, k)$, with the calculated filter coefficients, $w(t, k)$. It can be seen that in the current implementation the Wiener filter requires only one parameters to be specified, C .

The spectral envelopes processed with the two designed filters are scaled by their standard deviation because unlike w_2 , w_1 can have negative values, when the scaled power of observed noise is larger than the scaled power of the observed signal for certain frequencies. The resultant signals are averaged to give a final spectral envelope of the cleaned PPG signal. The dominant frequency (the frequency with the highest magnitude) is converted to the HR estimate in BPM as shown in Fig. 3(c).

C. HR Estimation and Refinement using Phase Vocoder.

In this work, the phase vocoder technique [32, 11–13] is employed to refine the initial HR estimate through the estimation of the instantaneous frequency as the rate of change of phase angle at time [33]. For signals that are not truly sinusoidal or for nonstationary signals one needs to account for the time-varying nature of the process and that can be done with estimation of the instantaneous frequency.

The effective frequency resolution (the minimum frequency that can be estimated, the Rayleigh frequency) of the data is limited by the size of the window of the analyzed data (8s) and equals to $1/8 \times 60 = 7.5$ BPM. Zero-padding before DFT is used to interpolate the spectral envelope to other frequencies thus decreasing the frequency spacing between neighboring DFT bins. This does not create new information but allows for a better revelation of the existing information in the signal.

The phase vocoder is the technique that is used in audio processing to manipulate audio length without changing its pitch or to change its pitch without affecting its length, by preserving the coherence of phase information. The phase vocoder uses a polar representation of the DFT and the instantaneous frequency estimation is computed as a discrete derivative of the phase. When analyzing the signal with multiple overlapping windows the individual signal components (sinusoids) will be correlated in time and spread over multiple adjacent DFT frequency bins (spectral leakage). The deviation of the true frequency from the bin center frequency is encoded in phase changes of two consecutive frames, so that the instantaneous frequency can be given as:

$$f(t) = \frac{1}{2\pi} \frac{d\theta(t)}{dt} \quad (6)$$

The DFT phases, θ_2 , θ_1 , from the current and previous frames, of the *chosen* frequency peak in the magnitude spectrum, f , are used to refine the initial frequency estimation:

$$\arg \min_n (\tilde{f}(n) - f); \tilde{f}(n) = \frac{(\theta_2 - \theta_1 + 2\pi n)}{(2\pi(t_2 - t_1))}, \forall n \in \mathbf{N} \quad (7)$$

where n is a positive integer, t_2 , t_1 are the time stamps of the two frames, here $t_2 - t_1 = 2s$ which is the window shift. The series, $\tilde{f}(n)$, is computed for several n using Eq. 7, and the value of \tilde{f} which is closest to the initial frequency estimation, f , is chosen. As a result, the previous dominant frequency value is refined to the new value, $f \leftarrow \tilde{f}$. This is illustrated in Fig. 3(d), where the estimated DFT HR of 161.3 BPM was refined to 158.2 BPM, with the true HR being of 159.1 BPM.

It can be seen that the phase vocoder technique requires no parameters to set.

D. Post-processing

1) Online post-processing with heuristic rules and thresholds

The post-processing steps include history tracking and smoothing. The history of the past HR estimation is preserved and used to guide the search range for the maximum DFT magnitude in the current frame. For instance, if the past HR estimation was 125 BPM, then the current HR is expected to be within a certain range around 125 BPM. Here it is set to the maximum absolute HR difference between consecutive HR estimates, $f(t)$, observed so far for this user:

$$\tau_i = \max\{|f(t) - f(t-1)|; k < t < i-1\} \quad (8)$$

The search range, $\pm \tau_i$, $t \leq k$ is initialized to be wide enough (± 25 BPM) for the first 30s – 1 min of each recording, and then adapts to the specifics of the user's physiology. This eliminates the need to tune another threshold in the post-processing.

For the final smoothing, the weighted average between the current estimate and its prediction using linear regression is computed if the difference between the current and previous HR estimates is above 5 BPM:

$$\tilde{f} = \alpha f + (1 - \alpha) f_{LinReg} \quad (9)$$

where f_{LinReg} is a prediction given by a regression line which is fitted over the past 6 HR estimates using a least-squares error, and $\alpha = 0.8$.

E. Offline post-processing with Viterbi decoding

The offline version of WFPV substitutes the original post-processing steps with a probabilistic framework using Viterbi decoding [28]. The time-frequency plane (spectrogram) of a complete recording which is composed of DFT magnitudes after Wiener filtering is considered as a N -by- T state-space map of emission probabilities, \mathbf{B} , for N states (discrete values of HR) and T observations (time windows), where b_{ji} is a magnitude

value of the j^{th} DFT bin for the t^{th} time window. The N -by- N matrix of transition probabilities, \mathbf{A} , where a_{ij} represents the probability of changing from the i^{th} HR to the j^{th} HR, is estimated from the ground truth automatically by counting the transitions using the leave-one-recording-out procedure. In this manner, the ground truth of the testing recording is never used but the ground truths of all other recordings are used to estimate the transition probability matrix. The process of estimation of the transition probability matrix is fully automatic, data-driven and requires no user-tunable parameters.

The Viterbi algorithm is then applied to recursively estimate the most likely path (the path with the highest cumulative probability) through the time dimension, t , using emission and transition probability matrices, \mathbf{B} , \mathbf{A} :

$$\Psi_t(j) = \underset{1 \leq i \leq N}{\operatorname{argmax}} [\delta_{t-1}(i) a_{ij}], \quad (10)$$

where $\delta_t(j) = \max_{1 \leq i \leq N} [\delta_{t-1}(i) a_{ij}] b_{jt}$, $2 \leq t \leq T$, $1 \leq j \leq N$, $\delta_1(i) = \pi_i b_{i1}$, $1 \leq i \leq N$, and π_i are the prior probabilities. After the recursion is computed the state sequence is backtracked as:

$$i_T = \underset{1 \leq i \leq N}{\operatorname{argmax}} [\delta_T(i)], \quad (11)$$

$$i_t = \Psi_{t+1}(i_{t+1}), t = T-1, T-2, \dots, 1$$

The state sequence is converted to HR estimates which are then smoothed with a non-causal (central) moving average filter. The Viterbi decoding effectively performs the post-processing in a threshold-free probabilistic manner.

The Matlab implementation of the online and offline WFPV HR estimators along with the main results are available online (<https://github.com/andtem2000/PPG>).

III. DATABASE & METRICS

A. Database

The data used were provided for the IEEE Signal Processing Cup 2015 and are detailed in Table I. The dataset consists of 23 5-min recordings which were collected from 18 to 58 years old subjects performing various physical exercises. For each subject, the PPG signals were recorded from the wrist using two PPG sensors with green LEDs (wavelength: 515nm). The acceleration signal was also recorded from the wrist using a three-axis accelerometer. Both the PPG sensors and the accelerometer were embedded in a comfortable wristband. The ECG signal was recorded simultaneously from the chest using wet ECG sensors. All signals were sampled at 125 Hz and sent to a nearby computer via Bluetooth.

Three types of activities were performed. Type 1 (T1) activity involved walking or running on a treadmill for intervals 0.5-1-1-1-0.5 min with the speed of 1-2 km/h, 6-8 km/h, 12-15 km/h, 6-8 km/h, 12-15 km/h, 1-2 km/h, respectively. The subjects were asked to use the hand with the wristband to pull clothes, wipe sweat on forehead, and push buttons on the treadmill. Type 2 activity included various forearm and upper arm exercises which are common in arm rehabilitation (e.g.

TABLE I
DATABASE OF 23 PPG RECORDINGS FROM IEEE SP CUP.

| Rec | Subject ID | Activity type* | Age/Weight/Height | Sex | Healthy? |
|-----|------------|----------------|-------------------|-----|----------|
| 1 | 1 | T1 | 18-35y/-/- | M | Y |
| 2 | 2 | T1 | | M | Y |
| 3 | 3 | T1 | | M | Y |
| 4 | 4 | T1 | | M | Y |
| 5 | 5 | T1 | | M | Y |
| 6 | 6 | T1 | | M | Y |
| 7 | 7 | T1 | | M | Y |
| 8 | 8 | T1 | | M | Y |
| 9 | 9 | T1 | | M | Y |
| 10 | 10 | T1 | | M | Y |
| 11 | 11 | T1 | | M | Y |
| 12 | 12 | T1 | | M | Y |
| 13 | 13 | T2 | 20y/64kg/162cm | M | Y |
| 14 | 14 | T2 | 29y/70kg/169cm | M | Y |
| 15 | 15 | T2 | 21y/77kg/188cm | M | Y |
| 16 | 15 | T3 | 21y/77kg/188cm | M | Y |
| 17 | 16 | T3 | 19y/54kg/174cm | M | Y |
| 18 | 13 | T3 | 20y/64kg/162cm | M | Y |
| 19 | 17 | T3 | 20y/57kg/174cm | M | Y |
| 20 | 18 | T2 | 19y/70kg/180cm | M | Y |
| 21 | 18 | T3 | 19y/70kg/180cm | M | Y |
| 22 | 19 | T3 | 21y/73kg/180cm | M | Y |
| 23 | 20 | T2 | 58y/70kg/156cm | F | N** |

* T1 = walking/running on a treadmill. T2 = rehabilitation arm exercises. T3 = intensive arm movements (boxing)

** Abnormal heart rhythm and blood pressure were noted.

shake hands, stretch, push, running, jump, and push-ups). Type 3 activity consisted of intensive forearm and upper arm movements (e.g. boxing).

The synchronously recorded ECG was used to provide the ground truth HR in BPM as described in detail in [2, 3]. The ECG-based HRs were calculated for every 8s window with a 2s shift. The same window length and shift are suggested for HR estimation from PPG to have the same number of HR estimates and true HRs. The ground truth HRs were then used to assess the performance of the developed algorithms.

B. Metrics

The metrics which are usually computed in other studies [3] are reported here. The Absolute Error (AE) is used to evaluate the accuracy of each HR estimate:

$$AE_i = |f_{est}(i) - f_{true}(i)| \quad (12)$$

where $f_{est}(i)$ and $f_{true}(i)$ denote the estimated and the true HR value in the i -th time window in BPM, respectively. The following three metrics are used to evaluate the performance of the developed algorithm, Average Absolute Error ($avAE$), Standard Deviation of the Absolute Error ($sdAE$) and Average Relative Error ($avRA$):

$$avAE = \frac{1}{N} \sum_{i=1}^N AE_i \quad (13)$$

$$sdAE = \sqrt{\frac{1}{N} \sum_{i=1}^N (AE_i - avAE)^2} \quad (14)$$

$$avRE = \frac{1}{N} \sum_{i=1}^N \frac{AE_i}{f_{true}(i)} \quad (15)$$

where N is the total number of estimates (number of windows).

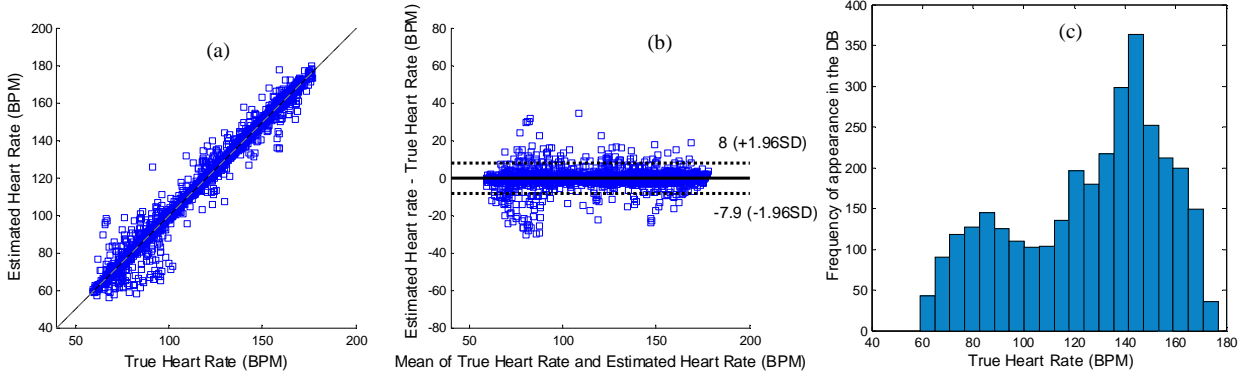


Fig. 4. (a) Pearson correlation between the estimated HR and the ground truth HR, (b) Bland-Altman plot, (c) the distribution of the HR in the DB. Correlation coefficient of the WFPV algorithm is 0.9908.

TABLE II.
PERFORMANCE OF WFPV.

| | | B | B&SS | B&WF1 | B&WF2 | B&WF1 & WF2 | B&WF&PV |
|-----|-------------|-------|------|-------|-------|-------------|-------------|
| All | <i>avAE</i> | 13.11 | 5.08 | 4.19 | 3.30 | 2.21 | 1.97 |
| | <i>sdAE</i> | 10.13 | 7.13 | 5.39 | 4.70 | 2.61 | 2.48 |

These metrics are reported for each of the 23 recordings.

IV. RESULTS AND DISCUSSION

A. Performance assessment

The performance of the proposed HR estimation system is summarized in Table II. On the database of 23 recordings, WFPV results in an *avAE* of 1.97 BPM with *sdAE* of 2.48 BPM. Table II also shows the contribution of each system constituent towards the final performance. The Baseline denotes the HR estimator as shown in Fig. 2, with all the preprocessing (filtering, normalization), DFT, and the post-processing (history tracking and smoothing), as described in Section III, but without Wiener filtering and the phase vocoder. The baseline is the system that takes the maximum DFT magnitude to determine the HR and has no routine to compensate for the presence of MA. The Baseline performance reaches an *avAE* of 13.11 BPM. If a simple spectral subtraction is added (Eq. 4, $C=1$), then the performance improves to 5.08 BPM (B&SS, Table II). Using the Wiener filter as described in Eq. 4 (WF1) improves the performance to 4.19 BPM. Using the recursive implementation of the Wiener filter (WF2) reduces the error from 5.08 to 3.30 BPM, and the combination of both filter, WF1 and WF2, results in an error of 2.21 BPM. A refinement introduced by the phase vocoder reduces the error to 1.97 BPM. A similar reduction in *sdAE* is observed.

Fig. 4 shows the correlation (a), Bland-Altman plot (b) and the distribution of HR in the database. Interestingly, Fig. 4(b) indicates that the largest errors (the points outside the limit of agreement area) occur more frequently in the low HR region, centered at ~ 80 BPM. At the same time, the most frequent HR according to Fig. 4(c) is much higher, ~ 140 BPM, but the algorithm makes fewer large errors in that region. This indicates the range of HR which are mostly affected by MA. Fig. 5 shows an example of the true and estimated HR for recording 9 – the recording with the best performance achieved.

Table III details the HR scores for each of the 23 recordings

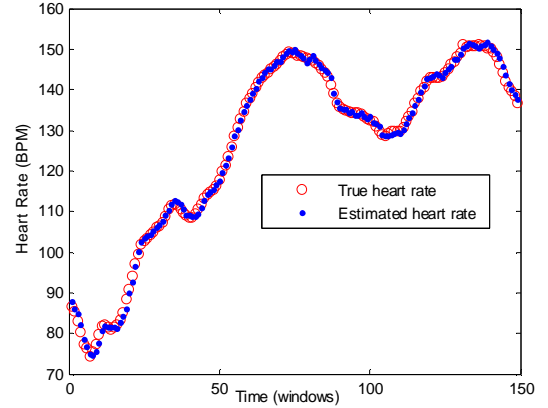


Fig. 5. The true and estimated heart rate for recording 9.

in the database, for *avAE* and *avRE* metrics, and also summarizes the performance for a group of recordings. It can be seen that the error in HR estimation heavily depends on the type of physical activity. Running on a treadmill results in an *avAE* of 1.02 BPM, whereas arm exercises and intensive arm exercises result in an *avAE* of 3.01 BPM, respectively.

B. Comparison with existing alternatives

Table III also provides the performance of alternative HR estimation algorithms tested on the same dataset or a part of it. Apart from TROIKA [2] and JOSS [3] the results are reported for several methods that have been recently published in journals such as: a time-varying spectral filtering algorithm for reconstruction of motion artifact (SpaMa, [21]), an algorithm based on ensemble empirical mode decomposition (EEMD, [23]), a HR estimation algorithm based on asymmetric least squares spectrum subtraction and Bayesian decision theory (Spectrap, [24]), an iterative method with adaptive thresholds (IMAT, [25]), and a multi-channel spectral matrix decomposition method [MC-SMD, 27].

The first 12 (T1 activity) of the 23 recordings of the dataset were used in [2] where the scores of 2.34, 1.82, and 2.47 BPM were reported for *avAE*, *avRE*, and *sdAE*, respectively. Subsequently, on the same dataset the *avAE* and *avRE* were reduced to 1.28 and 1.01 BPM, with an increased *sdAE* of 2.61 BPM in [3]. Evaluating on the same 12 recordings, the developed system obtains scores of 1.02, 0.81 and 1.25 BPM for *avAE*, *avRE*, and *sdAE*, respectively, which corresponds to

TABLE III.
COMPARISON OF THE HR ESTIMATION ERRORS ON 23 PPG RECORDINGS OF VARIOUS ALGORITHMS PROPOSED IN THE LITERATURE.

| Rec | Activity | | TROIKA* [2] | JOSS* [3] | SpaMa [21] | EEMD [23] | Spectrap [24] (Offline) | IMAT [25] | MC-SMD [27] | WFPV This study | WFPV+VD This study (Offline) |
|------|-----------------|------|----------------|--------------|---------------|--------------|-------------------------------|--------------|----------------|--------------------|------------------------------------|
| 1 | T1 | | 2.29 2.18 | 1.33 1.19 | 1.23 1.14 | 1.70 - | 1.18 1.04 | 1.72 1.50 | 1.16 0.91 | 1.25 1.15 | 0.93 0.89 |
| 2 | T1 | | 2.19 2.37 | 1.75 1.66 | 1.59 1.30 | 0.84 - | 2.42 2.33 | 1.33 1.30 | 1.07 0.87 | 1.41 1.30 | 0.82 0.73 |
| 3 | T1 | | 2.00 1.50 | 1.47 1.27 | 0.57 0.45 | 0.56 - | 0.86 0.66 | 0.90 0.75 | 0.80 0.62 | 0.71 0.59 | 0.64 0.54 |
| 4 | T1 | | 2.15 2.00 | 1.48 1.41 | 0.44 0.31 | 1.15 - | 1.38 1.31 | 1.28 1.20 | 1.13 0.84 | 0.97 0.88 | 0.83 0.80 |
| 5 | T1 | | 2.01 1.22 | 0.69 0.51 | 0.47 0.31 | 0.77 - | 0.92 0.74 | 0.93 0.69 | 0.98 0.68 | 0.75 0.57 | 0.50 0.38 |
| 6 | T1 | | 2.76 2.51 | 1.32 1.09 | 0.61 0.45 | 1.06 - | 1.37 1.14 | 1.41 1.20 | 1.29 0.96 | 0.92 0.75 | 0.78 0.61 |
| 7 | T1 | | 1.67 1.27 | 0.71 0.54 | 0.54 0.40 | 0.63 - | 1.53 1.36 | 0.61 0.50 | 0.88 0.65 | 0.65 0.50 | 0.50 0.40 |
| 8 | T1 | | 1.93 1.47 | 0.56 0.47 | 0.40 0.33 | 0.53 - | 0.64 0.55 | 0.88 0.80 | 0.81 0.64 | 0.97 0.83 | 0.67 0.56 |
| 9 | T1 | | 1.86 1.28 | 0.49 0.41 | 0.40 0.42 | 0.52 - | 0.60 0.52 | 0.59 0.50 | 0.55 0.43 | 0.55 0.48 | 0.45 0.38 |
| 10 | T1 | | 4.70 2.49 | 3.81 2.43 | 2.63 1.59 | 2.56 - | 3.65 2.27 | 3.78 2.40 | 3.18 1.95 | 2.06 1.29 | 1.43 0.90 |
| 11 | T1 | | 1.72 1.29 | 0.78 0.51 | 0.64 0.42 | 1.05 - | 0.92 0.65 | 0.85 0.60 | 0.79 0.51 | 1.03 0.68 | 0.74 0.48 |
| 12 | T1 | | 2.84 2.30 | 1.04 0.81 | 1.20 0.86 | 0.91 - | 1.25 1.02 | 0.71 0.50 | 0.72 0.53 | 0.99 0.70 | 0.75 0.53 |
| 13 | T2 | | - | - | 3.41 4.25 | - | - | - | - | 3.54 4.08 | 2.77 3.19 |
| 14 | T2 | | 6.63 8.76 | 8.07 10.9 | 7.29 9.80 | - | 4.89 6.29 | - | - | 9.59 12.2 | 8.68 10.9 |
| 15 | T2 | | 1.94 2.56 | 1.61 2.01 | 2.73 2.21 | - | 1.58 1.98 | - | - | 2.57 3.16 | 1.99 2.43 |
| 16 | T3 | | 1.35 1.04 | 3.10 2.69 | 3.18 2.11 | - | 1.83 1.49 | - | - | 2.25 1.87 | 1.83 1.51 |
| 17 | T3 | | 7.82 4.88 | 7.01 4.49 | 3.01 2.52 | - | 3.05 2.00 | - | - | 3.01 1.99 | 2.22 1.49 |
| 18 | T3 | | 2.46 2.00 | 2.99 2.52 | 4.46 3.23 | - | 1.62 1.36 | - | - | 2.73 2.29 | 2.01 1.70 |
| 19 | T3 | | 1.73 1.27 | 1.67 1.23 | 3.58 3.98 | - | 1.24 0.92 | - | - | 1.57 1.15 | 1.23 0.90 |
| 20 | T2 | | 3.33 3.90 | 2.80 3.46 | 1.94 1.66 | - | 2.04 2.23 | - | - | 2.10 2.41 | 1.53 1.78 |
| 21 | T3 | | 3.41 2.43 | 1.88 1.32 | 2.56 2.02 | - | 2.49 1.81 | - | - | 3.44 2.45 | 2.74 1.96 |
| 22 | T3 | | 2.69 2.12 | 0.92 0.74 | 3.12 3.28 | - | 1.16 0.92 | - | - | 1.61 1.26 | 1.02 0.80 |
| 23 | T2 | | 0.51 0.59 | 0.49 0.57 | 1.72 1.97 | - | 0.66 0.79 | - | - | 0.75 0.88 | 0.51 0.59 |
| Mean | T1 | avAE | 2.34 | 1.28 | 0.89 | 1.02 | 1.50 | 1.25 | 1.11 | 1.02 | 0.65 |
| | Rec 1-12 | avRE | 1.82 | 1.01 | 0.65 | - | 1.12 | 0.99 | 0.80 | 0.81 | 0.55 |
| | | sdAE | 2.47 | 2.61 | - | 1.79 | 1.95 | - | 1.99 | 1.25 | 1.00 |
| | | | | | | | | | | | |
| | T2-T3 | avAE | - | - | 3.36 | - | - | - | - | 3.01 | 2.16 |
| | Rec 13-23 | avRE | - | - | 3.33 | - | - | - | - | 3.06 | 2.21 |
| | | sdAE | - | - | - | - | - | - | - | 3.83 | 2.89 |
| | | | | | | | | | | | |
| | Test | avAE | 3.19 | 3.05 | 3.35 | - | 2.13 | - | - | 2.95 | 2.11 |
| | Rec 14-23 | avRE | 2.95 | 3.00 | 3.27 | - | 2.77 | - | - | 2.96 | 2.12 |
| | | sdAE | 3.61 | 3.35 | - | - | 2.04 | - | - | 3.71 | 2.82 |
| | | | | | | | | | | | |
| | Rec 1-12, 14-23 | avAE | 2.73 | 2.08 | 2.01 | - | 1.79 | - | - | 1.90 | 1.31 |
| | | avRE | 2.33 | 1.91 | 1.84 | - | 1.87 | - | - | 1.98 | 1.26 |
| | | sdAE | 2.99 | 2.79 | - | - | 1.99 | - | - | 2.37 | 1.83 |
| All | Rec 1-23 | avAE | - | - | 2.07 | - | - | - | - | 1.97 | 1.37 |
| | | avRE | - | - | 1.95 | - | - | - | - | 1.89 | 1.34 |
| | | sdAE | - | - | - | - | - | - | - | 2.48 | 1.91 |

* The HRs generated by TROIKA and JOSS on recordings 14-23 are obtained from <https://sites.google.com/site/researchbyzhang/publications>.

TABLE IV.
THE NUMBER OF USER-TUNABLE PARAMETERS.

| # tunable thresholds | TROIKA [2] | JOSS [3] | SpaMa [21] | EEMD [23] | Spectrap [24] | IMAT [25] | MC-SMD [27] | WFPV This study | WFPV+VD This study |
|----------------------------|---------------|-------------|---------------|--------------|------------------|--------------|----------------|--------------------|-----------------------|
| De-noising & HR detection* | >10 | 5 | 6 | >10 | 6 | >10 | >10 | 2 | 2 |
| Post-processing | >10 | >10 | 5 | >10 | 4 | >10 | >10 | 4 | 1 |

* The number of parameters does not include the preprocessing parameters such as filter length, cut-off points, down-sampling, etc.

a relative error reduction of 20% and 52% for *avAE* and *sdAE*. It can be seen that the error was significantly reduced for the worst performing recordings in the dataset which is reflected in the lower *sdAE*. The correlation coefficient was 0.997, as compared to 0.993 in [3]. On the first 12 PPG recordings the WFPV algorithm outperforms all of the listed approaches with the exception of SpaMa [21].

On the last 10 PPG recordings (rec. 14-23), WFPV also outperforms all the listed approaches including SpaMa [21] with the exception of Spectrap [24] which employs non-causal smoothing and cannot be seen as an online algorithm. Because

most studies do not report results for rec. 13, the majority of approaches can be compared using the average of the results for rec. 1-12 and 14-23. With an *avAE* of 1.90 BPM, the proposed approach outperforms all the listed alternatives.

Looking at the performance of the offline version (WFPV+VD), it can be seen that the incorporation of Viterbi decoding and non-causal smoothing has a significant effect on the performance, reducing the *avAE* from 1.97 to 1.37 BPM, outperforming all the listed methods including the offline Spectrap [24]. This indicates that the performance comparison is only sensible among the algorithms that perform either

offline or online processing.

C. Analysis

The approaches reported in [2, 3, 23, 24, 25, 27] rely on a number of heuristic rules and thresholds (Table IV). For instance, the post-processing step alone in [2, 3, 23, 27] requires a dozen parameters to be specified. The relevance of the knowledge extracted from the data (in terms of the rules and threshold values) is tested on the same data and the best achievable results are usually reported. Increasing the number of degrees of freedom of the designed system will inevitably lead to an improved performance but it comes at the cost of an increased risk of poor generalization on the unseen data, especially if fine-tuning is performed in the post-processing to correct the errors of the core algorithm.

As can be seen from Table III, some studies report results only on the first 12 recordings (T1 activity); others in addition report performance on the data that were used as test data in SP Cup (rec. 14-23), and only a few report the performance on the whole dataset of all 23 recordings. It is worth noting that since the ground truth for the whole dataset is available, there is no difference between the training and testing data from the performance assessment perspective. In this context, the number of the free parameters of the developed system is the only indicator of the potential overfit. It can also be seen from Table III that although the whole database of 23 recordings is available since early 2015, several very recent works [23, 25, 27] still prefer to report results on the ‘easier’ part of the dataset, T1 activity only.

The method presented in this study requires only a few parameters to be tuned. The number of frequency bins in the DFT was set to 1024 (with zero-padding). Likewise, $C=15$ was used in the Wiener filters. The range of the search space for the maximum in DFT magnitudes for the next frame is determined adaptively using Eq. 8. Viterbi decoding for the offline algorithm does not require any thresholds to tune. The proposed algorithm takes under 10s to process the whole PPG dataset of 23 recordings (Matlab R2013b @ Intel Core E7200 2.5GHz) which compares favorably with techniques reported in [2, 3, 22, 23, 25]. It is reported in [23] that in order to estimate the HR for the first 12 recordings TROIKA [2] takes several hours, JOSS [3] takes 300s, EEMD [23] takes 200s, and IMAT [25] takes several hours as tested in this study using the provided implementation.

Reproducibility is an essential principle of the scientific process. The availability of the data and the algorithm code will encourage more researchers to explore the area of PPG signal processing and build novel technical solutions. Unfortunately, among the solutions discussed in Table III only the implementation of the IMAT algorithm [25] is available online. Reproducibility of results will allow for verification of genuine technical contributions.

D. Combination with other approaches

It is well known that a better performance can be obtained by blending complementary approaches [34]. Table V shows the performance of the system that ensembles the TROIKA [2],

TABLE V.
PERFORMANCE OF THE ENSEMBLE OF THE THREE HR ESTIMATION
ALGORITHMS ON RECORDINGS 14-23.

| | | TROIKA[2] | JOSS [3] | WFPV | Ensemble |
|---------------|-------------|-----------|----------|------|-------------|
| Rec. 14-23 | <i>avAE</i> | 3.19 | 3.05 | 2.95 | 2.32 |
| | <i>avRE</i> | 2.95 | 3.00 | 2.96 | 2.29 |
| | <i>sdAE</i> | 3.61 | 3.35 | 3.71 | 2.37 |

JOSS [3] and WFPV methods by taking a simple average of their HR estimates. It can be seen that even a late decision-level combination of the HR estimates significantly reduces the error in all reported metrics. In fact, Bland-Altman plots that show the distribution of errors for a given algorithm (as shown in Fig. 4(b) for WFPV) can be used to assess the level of complementarity of various approaches – for instance, algorithms that produce most errors in the region of high HR would be good candidates to form ensemble with WFPV. For this purpose, the availability of the algorithms implementation for building more accurate solutions is essential.

V. CONCLUSIONS

An algorithm based on the Wiener filtering and the phase vocoder is proposed. It provides a simple but effective solution to the PPG-based HR estimation and can serve as a baseline performance for further studies. The algorithm has low computational cost and is well suited for fitness tracking and health monitoring in wearable devices [18, 19]. An offline version of the algorithm with a higher accuracy is proposed that utilizes Viterbi decoding to post-process HR estimates. The Matlab implementation for both algorithms is provided.

Future research may concentrate on the usage of other spectral estimation methods. The Wiener filter can be applied in the time domain to facilitate this option. Additionally, prior information available about the user, such as the user weight or age may be incorporated to estimate the maximum HR expected. The probabilistic framework with Viterbi decoding can be adapted to online monitoring with a predefined delay. Finally, electric potential wearable sensors can be used to complement the PPG ones [35].

REFERENCES

- [1] J. Allen, “Photoplethysmography and its application in clinical physiological measurement,” *Phys Meas*, v. 28, pp. 1-39, 2007.
- [2] Z. Zhang, Z. Pi, B. Liu, “TROIKA: A General Framework for Heart Rate Monitoring Using Wrist-Type Photoplethysmographic Signals During Intensive Physical Exercise,” *IEEE Trans Biomed Eng*, v. 62, pp. 522-531, 2015.
- [3] Z. Zhang, “Photoplethysmography-Based Heart Rate Monitoring in Physical Activities via Joint Sparse Spectrum Reconstruction,” *IEEE Trans Biomed Eng*, v.62, pp. 1902-1910, 2015.
- [4] R. Yousefi, M. Nourani, S. Ostadabbas, and I. Panahi, “A motion-tolerant adaptive algorithm for wearable photoplethysmographic biosensors,” *IEEE J Biomed Health*, v. 18, pp. 670-681, 2014.
- [5] M. Ram, K. V. Madhav, E. H. Krishna, N. R. Komalla, and K. A. Reddy, “A novel approach for motion artifact reduction in PPG signals based on AS-LMS adaptive filter,” *IEEE Trans Instrum Meas*, v. 61, pp. 1445-1457, 2012.
- [6] B. Kim, S. Yoo, “Motion artifact reduction in photoplethysmography using independent component analysis,” *IEEE Trans Biomed Eng*, v. 53, pp. 566-568, 2006.
- [7] X. Sun, P. Yang, Y. Li, Z. Gao, and Y.-T. Zhang, “Robust heart beat detection from photoplethysmography interlaced with motion artifacts

- based on empirical mode decomposition,” in Proc. IEEE BHI, pp. 775–778, 2012.
- [8] H. Fukushima, H. Kawanaka, M. Bhuiyan, and K. Oguri, “Estimating heart rate using wrist-type photoplethysmography and acceleration sensor while running,” in Proc. IEEE EMBC, pp. 2901–2904, 2012.
 - [9] B. Lee, J. Han, H. Baek, J. Shin, K. Park, and W. Yi, “Improved elimination of motion artifacts from a photoplethysmographic signal using a kalman smoother with simultaneous accelerometry,” *Physiol Meas*, vol. 31, no. 12, pp. 1585–1603, 2010.
 - [10] S. Cotter, B. Rao, K. Engan, and K. Kreutz-Delgado, “Sparse solutions to linear inverse problems with multiple measurement vectors,” *IEEE Trans Signal Process*, v. 53, pp. 2477–2488, 2005.
 - [11] J. Flanagan, R. Golden, “Phase Vocoder,” Bell System Technical Journal, 1493-1509, 1966.
 - [12] T. Dutoit, F. Marqués. Applied Signal Processing – A MATLAB-Based Proof of Concept. Springer, 2009.
 - [13] A. Temko, W. Marnane, G. Boylan, G. Lightbody, “Clinical Implementation of a Neonatal Seizure Detection Algorithm,” *Decis Support Syst*, v.70, pp. 86–96, 2015.
 - [14] Z. Zhang “Heart Rate Monitoring from Wrist-Type Photoplethysmographic (PPG) Signals During Intensive Physical Exercise,” In Proc. GlobalSIP, pp. 866-870, 2014.
 - [15] R. Brown, P. Hwang. *Introduction to Random Signals and Applied Kalman Filtering* (3 ed.). New York: John Wiley & Sons, 1996.
 - [16] S. Boll, “Suppression of Acoustic Noise in Speech Using Spectral Subtraction,” *IEEE Trans Acoust Speech Signal Process*, v. 27, 1979.
 - [17] A. Temko, G. Boylan, W. Marnane, G. Lightbody, “Robust Neonatal EEG Seizure Detection Through Adaptive Background Modelling,” *Int J Neural Syst*, v. 23, i. 4, World Scientific, 2013.
 - [18] M. Magno, C. Spagnol, L. Benini, E. Popovici, “Wearable Low Power Dry Surface Wireless Sensor Node for Healthcare Monitoring Application”, in Proc. IEEE 9th International Conference on Wireless and Mobile Computing, pp. 200-206, 2013.
 - [19] A. Temko, R. McEvoy, D. Dwyer, S. Faul, G. Lightbody, W. Marnane, “REACT: Real-Time EEG Analysis for Event Detection,” in Proc. AMA-IEEE Medical Technology Conf. on Individualized Healthcare, 2010.
 - [20] A. Temko, “Estimation of Heart Rate from Photoplethysmography during Physical Exercise using Wiener Filtering and the Phase Vocoder,” in Proc. IEEE EMBC, Aug. 2015.
 - [21] S. Salehizadeh, D. Dao, J. Bolkhovsky, C. Cho, Y. Mendelson, K. Chon, “A Novel Time-Varying Spectral Filtering Algorithm for Reconstruction of Motion Artifact Corrupted Heart Rate Signals During Intense Physical Activities Using a Wearable Photoplethysmogram Sensor,” *Sensors*, 16(1), 2016.
 - [22] H. Pan, D. Temel, G. AlRegib, “HeartBEAT: Heart beat estimation through adaptive tracking,” in Proc. IEEE EMBC, 2016.
 - [23] E. Khan, F. Al Hossain, S. Uddin, S. Alam, M. Hasan, “A Robust Heart Rate Monitoring Scheme Using Photoplethysmographic Signals Corrupted by Intense Motion Artifacts,” *IEEE Trans Biomed Eng*. v.63, pp. 550-562, 2016.
 - [24] B. Sun, Z. Zhang, “Photoplethysmography-based heart rate monitoring using asymmetric least squares spectrum subtraction and bayesian decision theory,” *IEEE Sensors J.*, v. 15, pp.7161-7168, 2015.
 - [25] M. Mashhadi, E. Asadi, M. Eskandari, S. Kiani, F. Marvasti, “Heart Rate Tracking using Wrist-Type Photoplethysmographic (PPG) Signals during Physical Exercise with Simultaneous Accelerometry”, *IEEE Signal Processing Letters*, v. 23, 2016.
 - [26] C. Garber, B. Blissmer, M. Deschenes, B. Franklin, et al., “Quantity and Quality of Exercise for Developing and Maintaining Cardiorespiratory, Musculoskeletal, and Neuromotor Fitness in Apparently Healthy Adults: Guidance for Prescribing Exercise,” *Med Sci Sports Exerc*, v. 43, pp. 1334-1359, 2011.
 - [27] J. Xiong, L. Cai, D. Jiang, H. Song, X. He, “Spectral Matrix Decomposition-Based Motion Artifacts Removal in Multi-Channel PPG Sensor Signals,” *IEEE Access*, 2016.
 - [28] L. Rabiner, “A tutorial on hidden Markov models and selected applications in speech recognition,” *Proc IEEE*, v. 77, pp. 257–286, 1989.
 - [29] A. Challoner, “Photoelectric plethysmography for estimating cutaneous blood flow. In *Non-invasive Physiological Measurement*; Rolfe, P., Ed.; Academic Press: Oxford, UK, v. 1, pp. 127–151, 1979.
 - [30] A. Kamal, J. Harness, G. Irving, A. Mearns, “Skin photoplethysmography – A review,” *Comput Methods Programs Biomed*, v. 28, pp. 257–269. 1989.
 - [31] S. Vaseghi, *Advanced Digital Signal Processing and Noise Reduction*, John Wiley & Sons, Ch 6, pp. 178-203, 2000.
 - [32] M. Puckette, J. Brown, “Accuracy of frequency estimate using the phase vocoder,” *IEEE Trans Speech Audio Process*, v. 6, pp. 166–176, 1998.
 - [33] B. Boashash, “Estimating and interpreting the instantaneous frequency of a signal. I. Fundamentals”, *Proc IEEE*, v. 80, pp. 520-538, 1992.
 - [34] E. Thomas, A. Temko, W. Marnane, G. Boylan, G. Lightbody, “Discriminative and generative classification techniques applied to automated neonatal seizure detection,” *IEEE J Biomed Health Informatics* v. 17 (2), 297-304, 2013.
 - [35] M. Magno, C. Spagnol, L. Benini, E. Popovici, “A low power wireless node for contact and contactless heart monitoring, *Microelectronics*, v. 45 (12), pp. 1656-1664, 2014.



Andriy Temko (M’05–SM’12) received the Engineering degree in Computer Science in 2002 from Dnipro National University, Dnipro, Ukraine and the PhD degree in Telecommunication in 2008 from Universitat Politècnica de Catalunya, Barcelona, Spain. During 2006-2007 he was a task leader in detection and classification of acoustic events within the EU-funded international evaluation campaigns on detection of events, activities, and their relationships. Since late 2008 he has been with the Irish Centre for Fetal and Neonatal Translational Research University College Cork, Ireland, working on algorithms for the detection of brain injuries in the newborn. He is the author of more than 70 peer-reviewed publications and 2 patents. He developed and patented a novel cutting-edge neonatal seizure detection system which is currently undergoing European multi-center clinical trial towards its regulatory approval and clinical adoption. In 2016 he was named as winner of the Kaggle challenge, and a \$10,000 first prize, for his work in predicting seizures in the human brain through long-term EEG recordings, organized by National Institute of Health, American Epilepsy Society and Melbourne University. His research interests include acoustic and physiological signal processing, clinical decision support tools, and applications of machine learning for signal processing.